ISSN 1392-1207. MECHANIKA. Vol. 30, No. 5, 2024: 398–407

Structure Analysis for Plate Components Using an Advanced Boundary Element Method

Yudong ZHONG, Xue ZENG, Guizhong XIE, Junjian HOU, Ruolan WANG, Liangwen WANG, Wenbin HE

Henan Provincial Key Laboratory of Intelligent Manufacturing of Mechanical Equipment, Mechanical and Electrical Engineering Institute, Zhengzhou University of Light Industry, Zhengzhou, 450002, Henan, China,
E-mail: zhongyd@zzuli.edu.cn

https://doi.org/10.5755/j02.mech.36578

1. Introduction

Due to the different structural properties of the plates used in various construction machinery structures, different characteristics have been formed, which determines their scope of use in actual projects. In the process of design and manufacture of mechanical structure and its components, the correct evaluation of its structural strength is a key technology. To ensure the normal use of the mechanical structures under various complex conditions, the related plate structures must have sufficient strength and fatigue resistance [1]. Accurately evaluating the strength of plate components can help to reduce the self-weight of mechanical structures, reduce the construction cost, improve the fatigue strength and the loading capacity, and thus improve the economy and safety of mechanical structure [2, 3]. So it is necessary to perform the structure analysis for plate components.

With the rapid development of computer technology and numerical theory, a great breakthrough has been made in the structure analysis of plate components by numerical methods. Among these numerical methods, Finite element method (FEM) is the most commonly used and greatly depends on the shape and quality of the mesh [4]. When FEM is used to analyze the thin plate components, the plate and shell elements with geometric assumptions are usually introduced [5]. If all solid elements are used, to avoid mesh distortion, a large number of meshes need to be divided according to the minimum feature size, resulting in a sharp increase in computation. Meshless methods [6-9] are developed which only need nodes without using predefined mesh information for domain discretization, and can easily simulate the flow field of various complex shapes by coordinate point calculation. Boundary element method (BEM) is a semi-analytical method, which has the advantages of dimensionality reduction and high computational accuracy [10-13]. In addition, BEM only needs boundary discretization and has no connectivity requirement for grid nodes, which is very suitable for analyzing the physical variables (e.g. displacement, traction, stress, etc.) of the plate components with thin features. In the boundary element analysis, to ensure the accurate calculation of the physical variables, the element interpolation and numerical integration (especially for the near singular integrals in thin-structural problems) associated with boundary integral equation (BIE) need special attention.

For element interpolation, at present, BEM mainly uses two interpolation methods: continuous element and discontinuous element interpolation [14]. The continuous element can reduce the discrete error of geometric model [15], while discontinuous element has the advantages of easy to handle corner and mesh generation [16, 17]. As BIE does not require the continuity of trial functions, the discontinuous element interpolation method is commonly used in the BEM analysis. However, discontinuous elements interpolation method cannot accurately simulate the physical quantities on small features and narrow surfaces of the plate components. Even if a large number of elements are placed on these special structures, it is difficult to achieve the desired effect, and the calculation amount also increases dramatically. To improve the simulation accuracy of physical variables on engineering structure, an advanced interpolation method is employed in this paper. The interpolation element is obtained by adding virtual points on the boundary of the original discontinuous element. As the degrees of freedom of virtual nodes can be eliminated by collocation nodes of the element, so the size of the coefficient matrix of the system equation is unchanged, and the order of interpolation polynomials is also improved.

In terms of numerical integration, there are both singular integrals and near singular integrals in the BIE due to the singularity of the fundamental solution. In structure analysis of BEM, there are several types of singular integrals in BIE, such as weakly singular and strongly singular integral. These types of singular integrals have been successfully evaluated by various methods, such as coordinate transformations method [18-20] and the approximate expansion methods [21, 22], etc. For near singular integrals, tremendous efforts have been made to derive convenient integral forms or construct complex transformation techniques, and good research achievements have been achieved. In these achievements, analytical and semi-analytical methods [23, 24], element subdivision [25, 26] and nonlinear transformation methods [27-31], etc. are included. As analytical integral methods and element subdivision methods are limited by generality and efficiency, nonlinear transformation methods are often employed to deal with the near singular integrals. In these nonlinear transformation methods, the sinh transformation method proposed by Johnston [32, 33] is an effective and general method to process near singular integrals. After this transformation, the trend of the integrand is smoothed and the near singularities can also be eliminated. Therefore, applying the sinh method, the near singular integrals in BIE of structure analysis for plate components with thin features can be accurately evaluated.

In this paper, an advanced BEM is developed to evaluate the physical variables for plate components with curve or thin features. Firstly, the expanding element

interpolation is employed to improve the simulation accuracy of the physical variables according to the characteristics of plate structure with curve or thin features, which can not only improve the order of interpolation polynomials without changing the degrees of freedom of system equations, but also can well simulate physical variables on curves and thin structures, reducing geometric errors. Then the integral transformation frame is applied to deal with the singular and near singular integral in BIE, to ensure the accurate calculation of the singular and near singular integrals on the geometrical model of plate components. With this method, the physical variables of the plate components can be accurately evaluated.

The outline of the paper as follows. Section 2 describes the numerical implementation of advanced BEM for structure analysis of plate components, which the treatment methods of element interpolation, singular and near singular integrals are included. A porous plate, a deck framing and a propeller structure are presented to verify the feasibility and universality of the presented method in Section 3. The conclusions are given in Section 4.

2. Numerical Implementation of the Advanced BEM

In the elastic structure analysis for the plate components, the corresponding equilibrium equations of this problem can be formulated in Eq. (1) [34] in the absence of the body forces.

$$\begin{aligned}
&\frac{2-2\nu}{1-2\nu}\frac{\partial^2 u_1}{\partial x_1^2}+\frac{\partial^2 u_1}{\partial x_2^2}+\frac{\partial^2 u_1}{\partial x_3^2}+\\
&+\frac{1}{1-2\nu}\frac{\partial^2 u_2}{\partial x_1\partial x_2}+\frac{1}{1-2\nu}\frac{\partial^2 u_3}{\partial x_1\partial x_3}=0,\\
&\frac{1}{1-2\nu}\frac{\partial^2 u_1}{\partial x_1\partial x_2}+\frac{\partial^2 u_2}{\partial x_1^2}+\\
&+\frac{2-2\nu}{1-2\nu}\frac{\partial^2 u_2}{\partial x_2^2}+\frac{\partial^2 u_2}{\partial x_3^2}+\frac{1}{1-2\nu}\frac{\partial^2 u_3}{\partial x_2\partial x_3}=0,\\
&\frac{1}{1-2\nu}\frac{\partial^2 u_1}{\partial x_1\partial x_3}+\frac{1}{1-2\nu}\frac{\partial^2 u_2}{\partial x_2\partial x_3}+\\
&+\frac{\partial^2 u_3}{\partial x_1^2}+\frac{\partial^2 u_3}{\partial x_2^2}+\frac{2-2\nu}{1-2\nu}\frac{\partial^2 u_3}{\partial x_3^2}=0.
\end{aligned}\tag{1}$$

in which, v denotes the Poisson's ratio, u_i is the component of displacement. For plane problem, i = 1, 2 and the variables in Eq. (1) associated with u_3 and x_3 are 0; for space problem, i = 1, 2, 3. The boundary conditions are given as follows

$$\text{Dirichlet: } u_i(x)=\bar{u}_i(x) \qquad x\in\Gamma_u, \tag{2}$$

$$\text{Neumann: } t_i(x)=\bar{t}_i(x) \qquad x\in\Gamma_t \tag{3}$$

in which, Γ denotes the boundary, t_i is the boundary traction. In BEM analysis for the plate components, the solutions of Eq. (1)-Eq. (3) can be solved by the BIE of the elasticity problem, and the formulas of the BIE can be expressed as [35]

$$\begin{aligned}
c_{ij}(P)u_j(P)=&\int_\Gamma u_{ij}^*(P,Q)t_j(Q)d\Gamma(Q)-\\
&-\int_\Gamma t_{ij}^*(P,Q)u_j(Q)d\Gamma(Q),
\end{aligned}\tag{4}$$

where $c_{ij}(P)$ is the free-term coefficients associated with the boundary Γ, P and Q are the source and field point in the discrete domain. u_j and t_j denote the displacement and traction on the boundary, respectively. $u_{ij}^*(P,Q)$ and $t_{ij}^*(P,Q)$ are the displacement and traction fundamental solutions which can be found in [39].

To evaluate the integral equation Eq. (4), the boundary Γ should be discretized first. If we discretize the boundary of the solution domain with N elements, the discrete equation can be formulated as

$$\begin{aligned}
c_{ij}(P)u_j(P)=&\sum_{e=1}^{N}\left\{\sum_{\alpha=1}^{n_e}t_j^\alpha\int_{\Gamma_e}u_{ij}^*(P,Q)N_\alpha(Q)d\Gamma(Q)\right\}-\\
&-\sum_{e=1}^{N}\left\{\sum_{\alpha=1}^{n_e}u_j^\alpha\right\}\int_{\Gamma_e}t_{ij}^*(P,Q)N_\alpha(Q)d\Gamma(Q)
\end{aligned}\tag{5}$$

in which, $N_\alpha(Q)$ is the shape function of the α^{th} node of the element Γ_e. It can be observed in Eq. (5), to evaluate the integral equation accurately and effectively, the element interpolation and numerical integration in Eq. (5) require special attention. Therefore, the paper focuses on the improvement of the interpolation and integration in integral equations of structure analysis for the plate components.

2.1. The implementation of element interpolation of advanced BEM

Due to the inevitable existence of narrow strip face, curved surface and other special structures in the plate structures, traditional element interpolation method cannot accurately simulate the physical quantities on these structures. Even if a large number of elements are placed on these special structures, it is difficult to achieve the desired effect and the computational efficiency will also decrease. In this section, a novel expanding element interpolation method is employed to improve the simulation accuracy of the physical quantities.

The interpolation element is composed of the source nodes and virtual nodes, and is obtained by adding virtual points on the boundary of the original discontinuous element. In the case of plane problem, the boundaries of a geometric model become line segments. Fig. 1 shows the three different types of line elements, where Fig. 1, a, Fig. 1, b, Fig. 1, c are the constant, linear and quadratic expanding element, respectively. The symbols s_i and v_i (i =1, 2, 3) in Fig. 1 represent the source and virtual nodes. It can be seen that the expanding element is similar to a continuous element and can raise the order of the interpolation polynomial. While the virtual nodes are removed, this element turns to be a discontinuous element. In this way, the expanding element has an ability to unify the discontinuous and continuous elements, and can better simulate the physical quantities on narrow faces and curved surface. The shape functions of the expanding element can be obtained by Lagrange interpolation according to the coordinates of its source and virtual points.

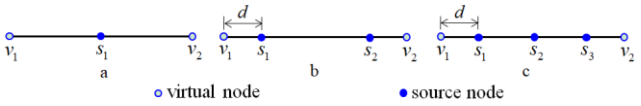

Fig. 1 Three types of expanding elements: a – constant expanding element; b – linear expanding element; c – quadratic expanding element

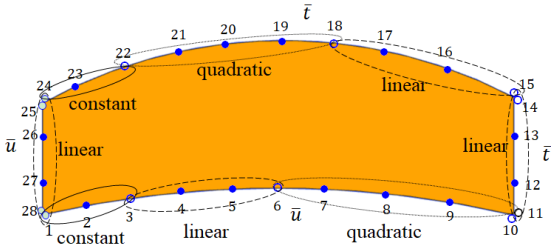

Fig. 2 The implementation example

In this element, the degrees of freedom of virtual nodes do not appear in the final system equation, so how to get the values of the virtual nodes is the key point. In the following part, the quadrilateral field with curve features in Fig. 2 is considered to introduce the computational method of the virtual nodes under different conditions. As shown in Fig. 2, the model is discretized into eight expanding elements, where two constant expanding elements, four linear expanding elements and two quadratic expanding elements are included.

The displacement boundary conditions $\bar{\boldsymbol{u}}$ are imposed on the bottom and left sides of the quadrilateral domain and the traction boundary conditions $\bar{\boldsymbol{t}}$ are applied on the bottom and right sides. The following content is the detailed interpolation process of the expanding element in the quadrilateral domain.

When interpolating the known variable on boundary, the value of the virtual node is directly equal to the boundary conditions. For example, the value of virtual nodes 22 and 6 in Fig. 2 can be can be directly equated to the boundary conditions $\bar{\boldsymbol{t}}$ of the side on which it is located. When interpolating the unknown variable on boundary, the values of virtual nodes can be obtained by extrapolating of adjacent elements and then averaging. Taking virtual nodes 6 and 18 in Fig. 2 as examples, the displacement boundary conditions of the edge where virtual node 6 is located are known, while the traction is unknown; and the traction boundary conditions of the edge where virtual node 18 is located are known, the displacement is unknown. The traction and displacement of the virtual nodes 6 and 18 can be obtained by Eq. (6)

$$\begin{aligned}\boldsymbol{t}_6 &= \frac{1}{2}\left[\left(N_4^r\boldsymbol{t}_4 + N_5^r\boldsymbol{t}_5\right) + \left(N_7^r\boldsymbol{t}_7 + N_8^r\boldsymbol{t}_8 + N_9^r\boldsymbol{t}_9\right)\right],\\ \boldsymbol{u}_{18} &= \frac{1}{2}\left[\left(N_{16}^r\boldsymbol{u}_{16} + N_{17}^r\boldsymbol{u}_{17}\right) + \left(N_{19}^r\boldsymbol{u}_{19} + N_{20}^r\boldsymbol{u}_{20} + N_{21}^r\boldsymbol{u}_{21}\right)\right].\end{aligned} \tag{6}$$

Here, N_i^r is the lower-order shape functions consisting of two internal source points of the element N_i^f is the higher-order shape functions consisting of the source points and virtual nodes. For the discontinuous traction field variables, two virtual points belong to the two adjacent elements of the connected vertices are configured at the geometric vertex of the boundary, which can ensure the accurate estimation of discontinuous boundary conditions. The traction values of virtual nodes 14 and 15 in Fig. 2 can be directly equated to the boundary conditions of the edge on which it is located (which is $\boldsymbol{t}_{14} = \bar{\boldsymbol{t}}_{14}$, $\boldsymbol{t}_{15} = \bar{\boldsymbol{t}}_{15}$). For continuous field variables, the value of virtual node at vertex 11 can be obtained by $\boldsymbol{u}_{11} = \boldsymbol{u}_{10} = \bar{\boldsymbol{u}}_{10}$, the virtual nodes 14 and 15 can be calculated by Eq. (7)

$$\begin{aligned}\boldsymbol{u}_{14} &= \boldsymbol{u}_{15} = \\ &= \frac{1}{2}\left(\left(N_{12}^r\boldsymbol{u}_{12} + N_{13}^r\boldsymbol{u}_{13}\right) + \left(N_{16}^r\boldsymbol{u}_{16} + N_{17}^r\boldsymbol{u}_{17}\right)\right).\end{aligned} \tag{7}$$

After the values of virtual nodes are obtained, the physical variables in the BIE can be interpolated by the high-order shape functions of the expanding element. The displacement and traction on the edge (such as right edge in Fig. 2) can be interpolated by Eq. (8).

$$\begin{cases}\boldsymbol{u} = N_{11}^f\boldsymbol{u}_{11} + N_{12}^f\boldsymbol{u}_{12} + N_{13}^f\boldsymbol{u}_{13} + N_{14}^f\boldsymbol{u}_{14}\\ \boldsymbol{t} = N_{11}^f\boldsymbol{t}_{11} + N_{12}^f\boldsymbol{t}_{12} + N_{13}^f\boldsymbol{t}_{13} + N_{14}^f\boldsymbol{t}_{14}\end{cases}. \tag{8}$$

Substituting the above method for solving virtual points into Eq. (8), the following expressions can be obtained

$$\begin{cases}\boldsymbol{u} = N_{11}^f\bar{\boldsymbol{u}}_{10} + \left(N_{12}^f + \frac{1}{2}N_{14}^fN_{12}^r\right)\boldsymbol{u}_{12} +\\ \quad + \left(N_{13}^f + \frac{1}{2}N_{13}^rN_{14}^f\right)\boldsymbol{u}_{13} +\\ \quad + \frac{1}{2}N_{14}^fN_{16}^r\boldsymbol{u}_{16} + \frac{1}{2}N_{14}^fN_{17}^r\boldsymbol{u}_{17},\\ \boldsymbol{t} = N_{11}^f\bar{\boldsymbol{t}}_{11} + N_{12}^f\bar{\boldsymbol{t}}_{12} + N_{13}^f\bar{\boldsymbol{t}}_{13} + N_{14}^f\bar{\boldsymbol{t}}_{14}\end{cases}. \tag{9}$$

By substituting the formulas of the above interpolation method to the discrete BIE, the integral forms in Eq. (5) can be rewritten as Eq. (10), and the n_e in Eq. (5) is the number of the element nodes (including source and virtual nodes).

$$\begin{cases}\boldsymbol{H}_{ij} = \int_{\Gamma_e}\boldsymbol{t}^*\left(P^i,Q\right)N_j^f\left(Q\right)d\Gamma\left(Q\right)\\ \boldsymbol{G}_{ij} = \int_{\Gamma_e}\boldsymbol{u}^*\left(P^i,Q\right)N_j^f\left(Q\right))d\Gamma\left(Q\right)\end{cases}. \tag{10}$$

Using Eq. (10), Eq. (5) can be rewritten as the matrix form $\boldsymbol{Hu} = \boldsymbol{Gt}$. If the computing domain is separated into n source nodes and m virtual nodes, the variables in the matrix are distinguished according to known and unknown boundary conditions, and the matrix equation can be expressed as

$$\begin{bmatrix} \bar{\boldsymbol{H}}^s & \boldsymbol{H}^s & \bar{\boldsymbol{H}}^v & \boldsymbol{H}^v \end{bmatrix} \begin{bmatrix} \bar{\boldsymbol{u}}^s \\ \boldsymbol{u}^s \\ \bar{\boldsymbol{u}}^v \\ \boldsymbol{u}^v \end{bmatrix} = \begin{bmatrix} \boldsymbol{G}^s & \bar{\boldsymbol{G}}^s & \boldsymbol{G}^v & \bar{\boldsymbol{G}}^v \end{bmatrix} \begin{bmatrix} \boldsymbol{t}^s \\ \bar{\boldsymbol{t}}^s \\ \boldsymbol{t}^v \\ \bar{\boldsymbol{t}}^v \end{bmatrix} \tag{11}$$

in which, the vectors $\bar{\boldsymbol{u}}$, $\bar{\boldsymbol{t}}$ and $\boldsymbol{u}$, $\boldsymbol{t}$ with the superscripts *s* and *v* denote the known and unknown boundary conditions at the source and virtual nodes, respectively. The matrixes $\bar{\boldsymbol{H}}$, $\bar{\boldsymbol{G}}$ and $\boldsymbol{H}$, $\boldsymbol{G}$ with the superscripts *s* and *v* are the composed of known and unknown quantities at the source and virtual nodes, respectively. Since the virtual nodes are not used as source points in Eq. (11), the matrices $\boldsymbol{H}$ and $\boldsymbol{G}$ are not square matrices. The values of the virtual nodes can be interpolated by the shape functions N_i^r of the corresponding elements, that is, by using the formulas $\boldsymbol{u}^v = \boldsymbol{N}^r \boldsymbol{u}^s$, $\boldsymbol{t}^v = \boldsymbol{N}^r \boldsymbol{t}^s$, the Eq. (11) can be further written as

$$\begin{bmatrix} \boldsymbol{H}^s + \boldsymbol{H}^v \boldsymbol{N}^r & -(\boldsymbol{G}^s + \boldsymbol{G}^v \boldsymbol{N}^r) \end{bmatrix} \begin{bmatrix} \boldsymbol{u}^s \\ \boldsymbol{t}^s \end{bmatrix} = \begin{bmatrix} \bar{\boldsymbol{G}}^s \bar{\boldsymbol{t}}^s + \bar{\boldsymbol{G}}^v \bar{\boldsymbol{t}}^v - \bar{\boldsymbol{H}}^s \bar{\boldsymbol{u}}^s - \bar{\boldsymbol{H}}^v \bar{\boldsymbol{u}}^v \end{bmatrix}. \tag{12}$$

According to Eq. (12), as the degrees of freedom of the virtual node can be condensed by the relationship with the source point, the size of the coefficient matrix of the linear system equation is the same as that of the traditional discontinuous element interpolation. Therefore, the presented method can improve the order of interpolation polynomials without changing the solution scale of system equations, and can better simulate the physical variables of the plate components.

2.2. The processing technique of boundary integrals in advance BEM

The plate structures contain skeleton plate, deck, and other thin structures. When BEM is used to analyze the physical variables of these structures, the singular integrals and a large number of near singular integrals will arise in the integral equation (Eq. (5) and Eq. (10)), we simplify this equation in the form of Eq. (13) (where $f(P, Q)$ is a regular term containing all external terms, such as shape functions, etc. r is the distance from the source point P to field point Q in boundary element). To ensure the simulative accuracy of the physical variables, the extra treatment of singular and near singular integrals is indispensable and this is also another key content of the paper.

$$\begin{aligned} I_1 &= \int_{\Gamma_e} f(P,Q) \ln r d\Gamma, \\ I_2 &= \int_{\Gamma_e} \frac{f(P,Q)}{r} d\Gamma. \end{aligned} \tag{13}$$

In terms of singular integrals, in can notice that the integral of displacement fundamental solution in Eq. (10) has $ln(1/r)$ singularity and the integral of traction fundamental solution has $1/r$ singularity. To remove the singularity in I_1, the weak singular integral can be formulated as the following form

$$I_1 = \int_{-1}^{1} f(\xi) ln\, r(\xi) d\xi = \int_{-1}^{1} f\left((\xi) - f(\eta)\right) ln\, r(\xi) d\xi + f(\eta) \int_{-1}^{1} ln\, r(\xi) d\xi, \tag{14}$$

where η is local coordinates of the field point Q related to the position of the source point, $f(\xi)$ is a regular term containing all external terms, such as the Jacobian of the coordinate transformation from the boundary element to local coordinates space [-1, 1], shape functions, etc. When P approaches Q, the local coordinate point ξ approaches η. The singularity in the first term of I_1 can be removed if $f(\xi)$ satisfies certain continuity conditions, such as the Lipschitz condition, and the second term of I_1 can be calculated straightforward by using the integral formula of integration by parts.

By using the above method, we can apply the subtraction and addition methods to eliminate the strong singularity in the integral I_2, and construct a formula $r_1(\xi)$ with the same properties as the integrand by performing a Taylor expansion of the distance function. The strong singular integral can be formulated as

$$\begin{aligned} I_2 &= \int_{-1}^{1} f(\xi) \frac{1}{r(\xi)} d\xi = \\ &= \int_{-1}^{1} \left(f(\xi) \frac{1}{r(\xi)} - \frac{f(\xi_0)}{r_1(\xi)} \right) d\xi + \int_{-1}^{1} \frac{f(\xi_0)}{r_1(\xi)} d\xi \end{aligned} \tag{15}$$

in which, ξ_0 is the local coordinate of the source point. With this equation, the singularity in the first term of I_2 can be removed, and the second term can be evaluated by analytic integral formulas.

In the current treatment of the near singular integrals, the sinh transformation methods [36, 37] are general methods to eliminate the near singularities. Take plane problem as the considered object, the near singular integrals arise in Eq. (10) and Eq. (13) can be rewritten as the following form

$$\begin{aligned} I_1 &= \int_{-1}^{1} f(\xi) \ln r(\xi) d\xi = \\ &= \frac{1}{2} \int_{-1}^{1} f(\xi) \ln((\xi - a)^2 + b^2) d\xi, \\ I_2 &= \int_{-1}^{1} f(\xi) \frac{1}{r(\xi)} d\xi = \\ &= \int_{-1}^{1} f(\xi) \frac{1}{\left((\xi - a)^2 + b^2\right)^l} d\xi. \end{aligned} \tag{16}$$

When P is close to the integral element Γ_e ($r \to 0$), the near singularity will arise. $l = 1/2$, $\xi \in [-1,1]$ is the local coordinates. The parameters a and b are the position of the projection of the source point and the shortest distance

between the source point and the boundary element, respectively (Fig. 3).

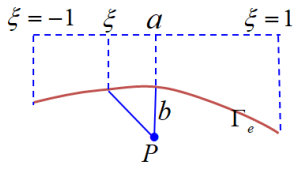

Fig. 3 The sketch map of near singular integrals

To evaluate the near singular integrals in Eq. (16), the following sinh transformation formula can be employed [40]

$$\xi = a + b\,sinh\left(k_1 t - k_2\right). \tag{17}$$

To facilitate the integration calculation with conventional Gaussian integrals, the interval of t can be selected as [-1, 1], and the variables k_1 and k_2 can be chosen

$$\begin{aligned} k_1 &= \frac{1}{2}\left[arcsin\,h\left(\frac{1+a}{b}\right) + arcsin\,h\left(\frac{1-a}{b}\right)\right], \\ k_2 &= \frac{1}{2}\left[arcsin\,h\left(\frac{1+a}{b}\right) - arcsin\,h\left(\frac{1-a}{b}\right)\right]. \end{aligned} \tag{18}$$

By using the transformation formula Eq. (17), the corresponding Jacobian of the sinh coordinate transformation can be obtained

$$\frac{d\xi}{dt} = bk_1\,cosh\left(k_1 t - k_2\right). \tag{19}$$

Substituting the transformation formula Eq. (17) and Eq. (19) into Eq. (16), the nearly singular integral formulas can be expressed as

$$\begin{aligned} I_1 &= \frac{bk_1}{2}\int_{-1}^{1} f(t)\,cosh\left(k_1 t - k_2\right)\cdot \\ &\quad \cdot ln\left(b^2\left(sinh^2\left(k_1 t - k_2\right)+1\right)\right)dt, \\ I_2 &= \frac{k_1}{b^{2l-1}}\int_{-1}^{1} f(t)\frac{cosh\left(k_1 t - k_2\right)}{\left(sinh^2\left(k_1 t - k_2\right)+1\right)^l}dt. \end{aligned} \tag{20}$$

With this transformation, the original integral kernels in Eq. (10) and Eq. (16) can be transformed into the well-behaved functions (see Eq. (20)). The near singularity of the integral kernels can be eliminated and the near singular integrals can be directly computed by using the regular Gaussian integrals. Therefore, the sinh method can remove the influence of near singular integrals in the BIE of structure analysis for plate components.

3. Numerical Examples

In this section, three plate structures with curve or thin features are given to verify the validity of the proposed method. In which, the symbols '*Exact_Tx*', '*Exact_Ty*' and '*Exact_Mises*' in all figures denote the analytical solution of traction in *x*, *y*, *z* direction and von Mises stress, respectively. The symbols '*Traditional_Tx*', '*Traditional_Ty*', '*Traditional_Mises*' and '*Proposed_Tx*', '*Proposed_Ty*', '*Proposed_Mises*' represent the numerical results obtained by traditional BEM and the advanced BEM, respectively.

3.1. The porous plate structure

To verify the validity and feasibility of the advanced method, a porous plate structure with 75 holes is considered in the first example, which is obtained by projective plane of deck plate. This structure can reduce weight and facilitate the access of maintenance personnel, which is widely used in the design and manufacture of engineering structures. As shown in Fig. 4, the length and width [2] of the porous plate are a = 2.4 m, b = 0.8 m, the transverse and longitudinal distance between the center of two adjacent holes are d = 0.15 m, c = 0.15 m. The radius of each hole is 0.02 m.

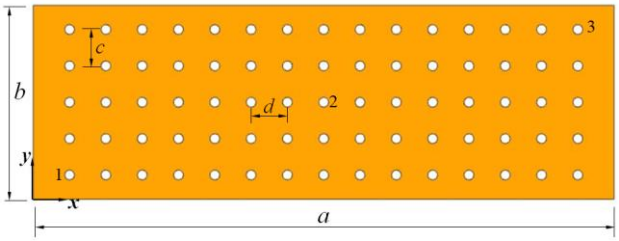

Fig. 4 The geometry of the porous plate structure

To compare with the analytical solutions, the secondary and cubic displacement analytical fields are imposed on the boundaries of the porous plate structure. The formulas of the analytical fields in Eq. (21) are given as follows:

$$\begin{aligned} &\text{secondary: } u_x = x^2 - 3y^2,\ u_y = -3x^2 + y^2, \\ &\text{cubic: } u_x = y^3 - 3yx^2,\ u_y = -x^3 + 3xy^2. \end{aligned} \tag{21}$$

The boundary of the geometric model of the porous plate structure is discretized into 332 quadratic elements. According to the geometrical and physical equations of elasticity, we can find the Young's modulus and Poisson's ratio only as a coefficient in the component of analytical solutions. So just for the sake of calculation, we assume the Young's modulus E = 1.0 and Poisson's ratio v = 0.25, respectively. Take the physical variables on circular holes *1*, *2* and *3* in Fig. 4 as the computational object. For a more intuitive comparison, the numerical results of tractions and von Mises stresses on the boundary of circle *1*, *2*, *3* are plotted on a graph, respectively, which are as shown in Fig. 5-Fig. 10. Where Fig. 5 and Fig. 9 are the numerical results on the boundary of the circle *1* with different boundary conditions, Fig. 6 and Fig. 10 are the numerical results on the boundary of the circle *2*, Fig. 7 and Fig. 10 are the numerical results on the boundary of the circle *3*. The X axes in Fig. 5-Fig. 10 represents the abscissa of the point on the circle *1*, *2* and *3*.

It can be observed from Fig. 5-Fig. 10, compared with the traditional boundary element method, whether it is a quadratic or a cubic analytical field, the results of the proposed method can agree very well with the analytical solution. Especially for the calculation of traction (e.g. *Tx*), when the traditional method is used to interpolate the

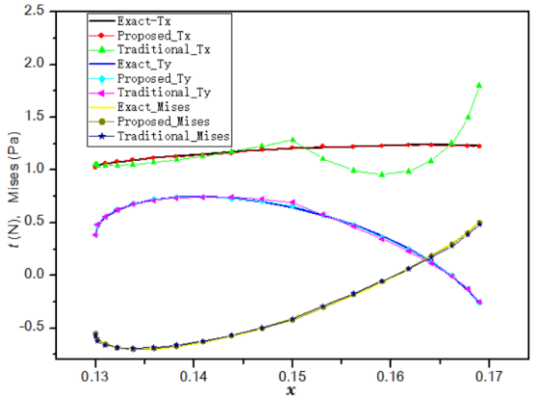

Fig. 5 The results on the boundary of the circle *1* with secondary fields

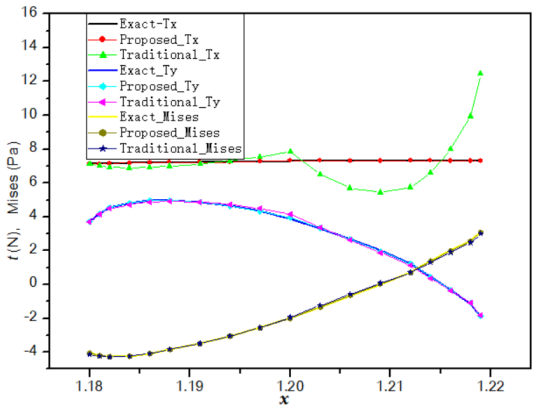

Fig. 6 The results on the boundary of the circle *2* with secondary fields

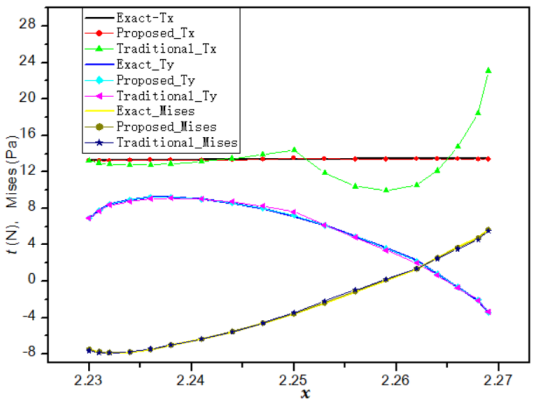

Fig. 7 The results on the boundary of the circle *3* with secondary fields

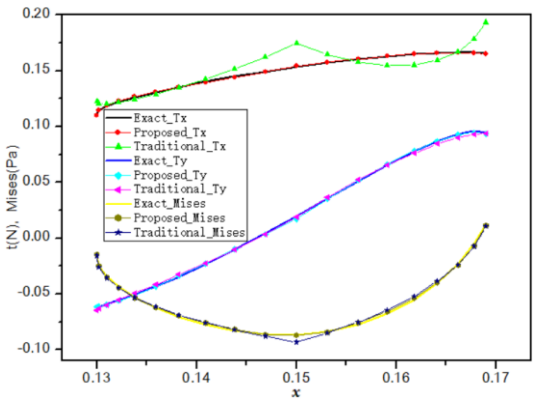

Fig. 8 The results on the boundary of the circle *1* with cubic field

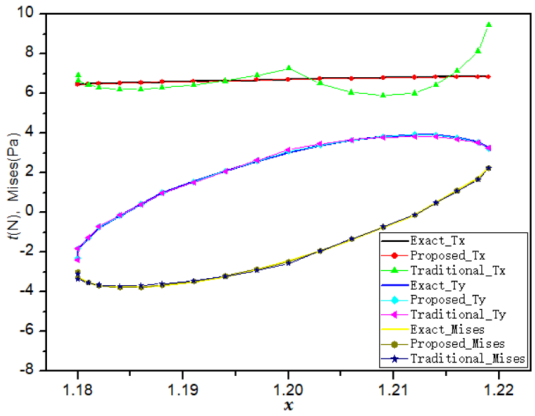

Fig. 9 The results on the boundary of the circle *2* with cubic field

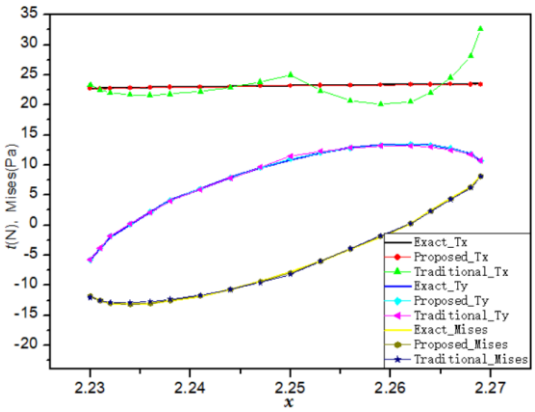

Fig. 10 The results on the boundary of the circle *3* with cubic field

physical variables on the curve features, to ensure the accuracy of the interpolation, a certain number of elements need to be used. However, when the number of elements is small, the interpolation accuracy of physical variables will be seriously affected, and the expanding element interpolation method used in the paper can overcome this defect, improve the interpolation accuracy without changing the size of the coefficient matrix of the system equation. In other words, with the same number of elements, the proposed method can obtain higher accuracy.

3.2. The deck framing

In this example, a cross-section of deck framing with thin features is considered to further verify the accuracy of the advanced method, which can be also seen as a stiffened plate of the panel structure. The coordinate system is located at the center of the deck framing model and the geometric parameters are as shown in Fig. 11, where the lengths a = 1.24 m, l = 0.6 m and the heights b = 2 m, h = 1 m, the thickness t = 0.02 m. For sake of calculation, the Young's modulus and Poisson's ratio are assumed to be $E = 1.0$, $v = 0.25$. In all boundaries of the deck framing structure, the cubic analytical fields in Eq. (22) are suffered as the boundary conditions.

$$u_x = y^3 - 3yx^2,\ u_y = -x^3 + 3xy^2,$$
$$\sigma_x = -4.8xy,\ \sigma_y = 4.8xy,\ \sigma_{xy} = 2.4\left(y^2 - x^2\right). \tag{22}$$

144 quadratic elements are used in the boundaries of the discrete geometric model. The advanced method is used to evaluate the physical variables of the deck framing structure. To compare with the analytical solutions, the numerical results on intraregional line *AB* (where $x = -0.31$), intraregional line *CD* (where $y = -0.51$), external Edge 1 and internal Edge 2 by using the proposed method are considered as the comparison objects, and the comparisons of results are shown in Fig. 12 – Fig. 15. Where the X axes in Fig. 12 and Fig. 14 represents the ordinates of the points on the line *CD* and Edge 1, the X axes in Fig. 13 and Fig. 15 represents the abscissas of the points on the line *AB* and Edge 2.

Fig. 12 – Fig. 17 show the results of the displacement and von Mises stress on line *AB* and *CD*, respectively. Fig. 16 and Fig. 17 show the results of the traction and von Mises

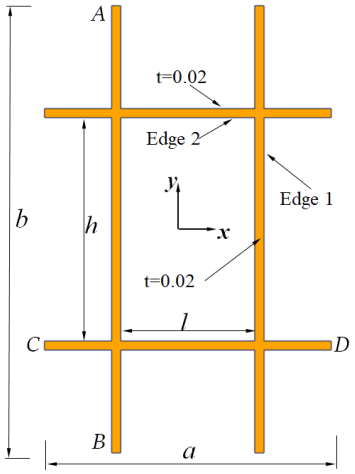

Fig. 11 The geometric model of the structure

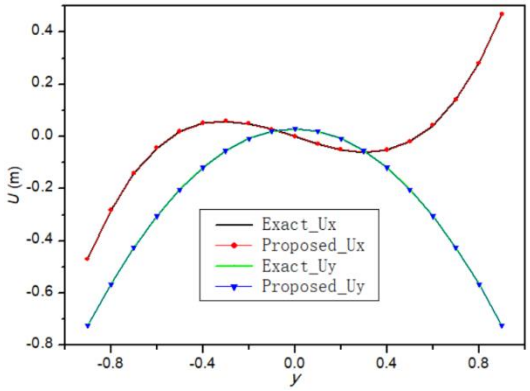

Fig. 12 The results of the displacement on the line *AB*

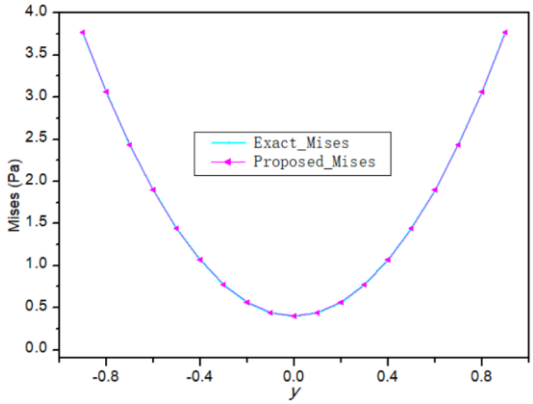

Fig. 13 The results of the von Mises stress on the line *AB*

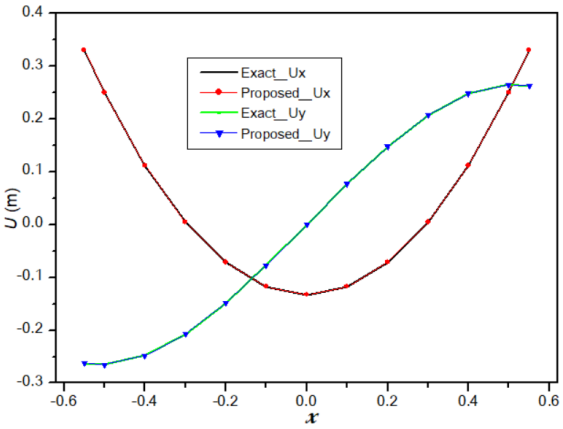

Fig. 14 The results of the displacement on the line *CD*

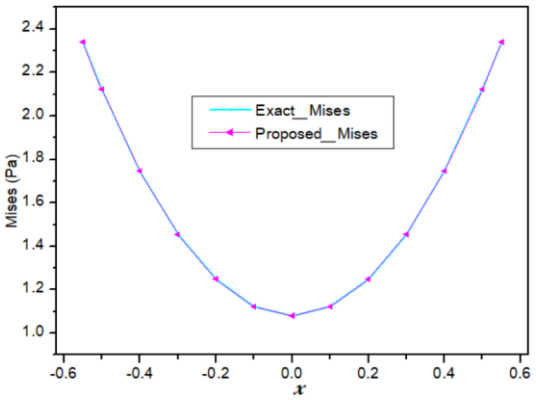

Fig. 15 The results of the von Mises stress on the line *CD*

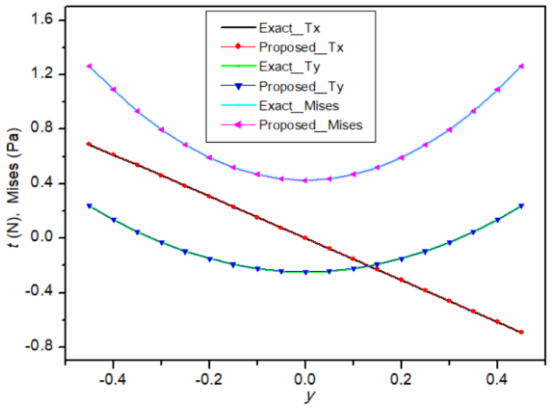

Fig. 16 The results of the traction and von Mises stress on the Edge 1

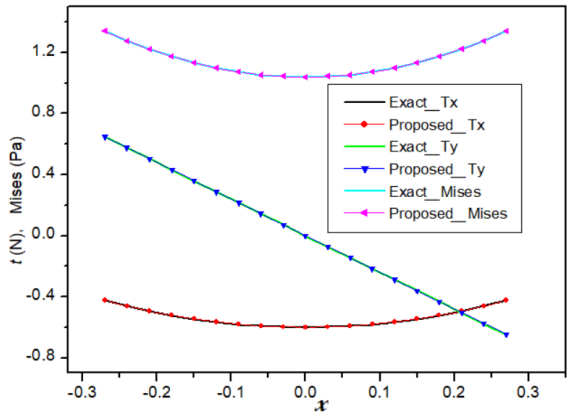

Fig. 17 The results of the traction and von Mises stress on the Edge 2

stress on Edge 1 and Edge 2, respectively. It can be seen from Fig. 12 – Fig. 17, the numerical results obtained by the advanced method can agree very well with the analytical solution, and the correctness of the presented method is further verified.

3.3. The propeller structure

To further verify the proposed method, a planar graph of the propeller with curve features is considered in Fig. 18. The geometrical parameters and the boundary conditions of the model are as shown in Fig. 18, a and Fig. 18, b, respectively, where $R1$ = 0.12 m, $R2$ = 0.274 m, $R3$ = 1.3769 m and P = 1 MPa. The Young's modulus E = 105 GPa, and the Poisson's ratio v = 0.25.

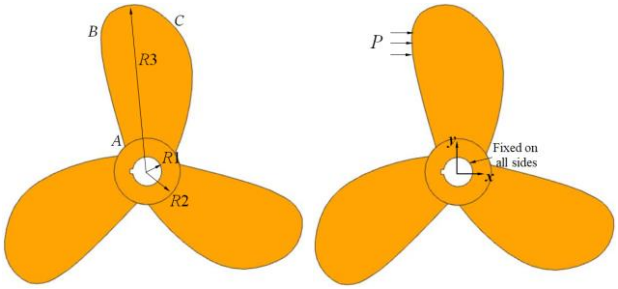

a b

Fig. 18 The Geometric model and boundary conditions

The boundary of the geometric model of the marine propeller is discretized into 132 quadratic elements, that is, the number of elements N in Eq. (5) is 132. The results obtained by finite element method with 6861 quadratic quadrilateral elements are regarded as the reference solution. The proposed method is employed to solve the integral equation Eq. (5), and the numerical results on the external boundary *AB* and *BC* together with the reference solution are shown in Fig. 19 – Fig. 22. The X axes in Fig. 19-Fig. 22 represents the abscissa of the point on the boundary *AB* and *BC*.

Fig. 19 and Fig. 20 illustrate the distributions of the displacement and von Mises stresses along the external boundary *BC*, respectively. Fig. 21 and Fig. 22 show the distributions of the displacement and Mises stresses along the external boundary *AB*, respectively. From Fig. 19 – Fig. 22, we can see the results obtained by the presented method can achieve the same effect as the reference solution obtained by FEM.

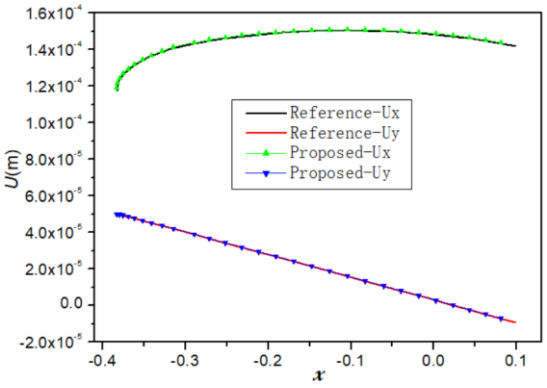

Fig. 19 The results on the boundary *BC*

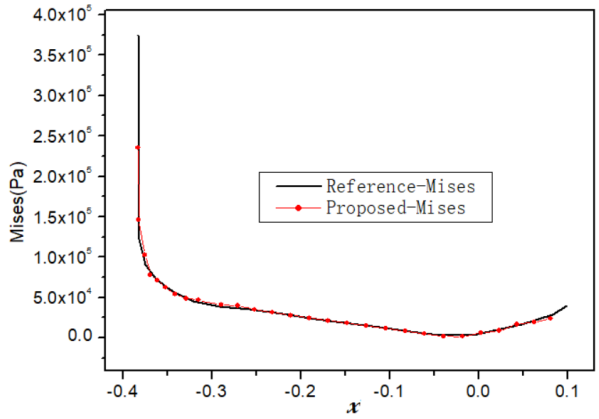

Fig. 20 The results of the Mises stress on the boundary *BC*

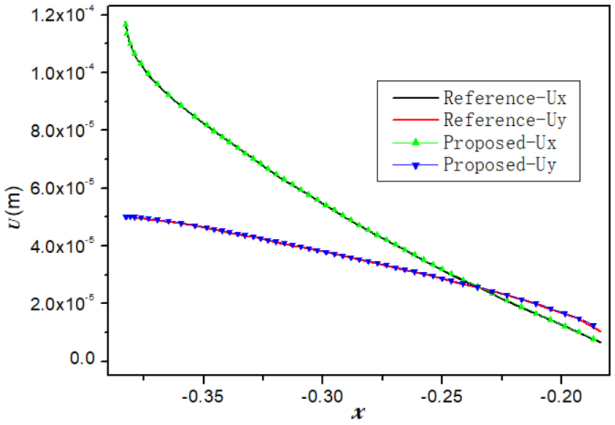

Fig. 21 The results on the boundary *AB*

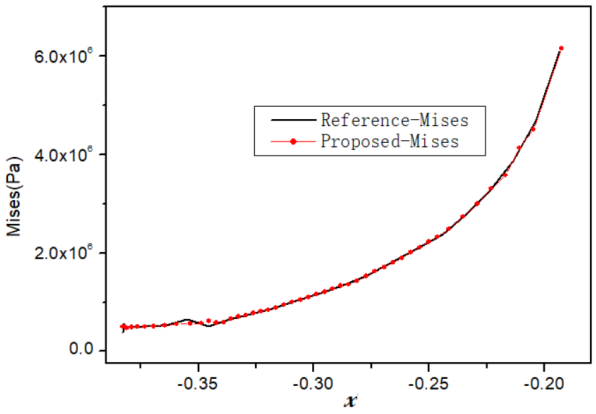

Fig. 22 The results of the Mises stress on the boundary *AB*

4. Conclusions

An advanced BEM is developed to perform structure analysis for plate components with curve or thin features. The advanced BEM first employs an expanding element interpolation method to improve the simulation accuracy of the physical quantities of the plate structures, which can improve the order of interpolation polynomials without changing the degrees of freedom of system equations; And then the integral frame is applied to deal with the singular and near singular integrals, to ensure the accurate calculation of elastic parameters. Finally, the advanced BEM is used to analyze the physical variables of plate components. The numerical results indicate that the advanced BEM can provide a precise and reliable solution for structural analysis,

and can be accurately and stably used for BEM analysis of plate components.

Acknowledgments

This work was partly supported by the National Natural Science Foundation of China (12302270), partly supported by the key scientific and technological project of Henan Province (232102221040 and 242102221003), and partly supported by Natural Science Foundation of Henan Province (232300420090), and partly supported by the Key Research and Development Projects in Henan Province (221111240200, 231111231200).

References

1. **Elosta, H.; Huang, S.; Incecik, A.** 2016. Significance of seabed interaction on fatigue assessment of steel catenary risers in the touchdown zone, Structural Engineering and Mechanics 57(3): 403-423. https://doi.org/10.12989/sem.2016.57.3.403.
2. **Tamboli, S.; Pandey, A.; Patil, M. V.** 2022. Investigation and optimisation of cracked aluminium alloy plate restored for fatigue loading application, International journal of computer aided engineering and technology 16(2): 153-169. http://doi.org/10.1504/IJCAET.2022.120832.
3. **Sajedin, A.; Shojaeifard, M., H.; Khalkhali, A**. 2019. Aero-Structural Study on the Blade Thickness Effects in an Automotive Turbocharger Turbine in Transonic Conditions, Mechanika 25(2): 134-140. https://doi.org/10.5755/j01.mech.25.2.22151.
4. **Morse, L.; Mallardo, V.; Aliabadi, F.** 2022. Manufacturing cost and reliability-based shape optimization of plate structures, International Journal for Numerical Methods in Engineering 123(10): 2189-2213. https://doi.org/10.1002/nme.6931.
5. **Grammatikopoulos, A.** 2021. The effects of geometric detail on the vibratory responses of complex ship-like thin-walled structures, Marine Structures 78(3): 103013. https://doi.org/10.1016/j.marstruc.2021.103013.
6. **Liu, Z. S.; Selim, B. A.** 2021.Impact analysis of functionally-graded graphene nanoplatelets-reinforced composite plates laying on Winkler-Pasternak elastic foundations applying a meshless approach, Engineering structures 241: 112453. https://doi.org/10.1016/j.engstruct.2021.112453.
7. **Feng, S. Z.; Han, X.; Ma, Z. J.; Królczyk, Z.; Li, Z.** 2020. Data-driven algorithm for real-time fatigue life prediction of structures with stochastic parameters, Computer Methods in Applied Mechanics and Engineering 372: 113373. https://doi.org/10.1016/j.cma.2020.113373.
8. **Zhong, Y. D.; Xie, G. Z.; Hou, J. J.; He, W.; Li, Y.** 2021. Thermal Elastic–Plastic Analysis of Three-Dimensional Structures Using Face-Based Smoothed Point Interpolation Method, International Journal of Computational Methods 18(8): 2150025. http://dx.doi.org/10.1142/S0219876221500250.
9. **Gu, Y.; Fan, C. M.; Xu, R. P.** 2019. Localized method of fundamental solutions for large-scale modeling of two-dimensional elasticity problems, Applied Mathematics Letters 93: 8-14. https://doi.org/10.1016/j.aml.2019.01.035.
10. **Zirakashvili, N.** 2020. Solution of Contact Problems for Half-Space by Boundary Element Methods Based on Singular Solutions of Flamant and Boussinesq's Problems, International Journal of Applied Mechanics 12(2): 2050015. https://doi.org/10.1142/S1758825120500155.
11. **Kostas, K. V.; Ginnis, A. I.; Politis, C. G.; Kaklis, P. D.** 2015. Ship-hull shape optimization with a T-spline based BEM–isogeometric solver, Computer Methods in Applied Mechanics and Engineering 284: 611-622. https://doi.org/10.1016/j.cma.2014.10.030.
12. **Sladek, J, Sladek, V.; Krivacek, J.; Aliabadi, M.** 2007. Local boundary integral equations for orthotropic shallow shells, International Journal of Solids and Structures 44(7-8): 2285-2303. https://doi.org/10.1016/j.ijsolstr.2006.07.010.
13. **Liu, Y. J.** 1998. Analysis of shell-like structures by the boundary element method based on 3-D elasticity: formulation and verification, International Journal for Numerical Methods in Engineering 41(3): 541-558. https://doi.org/10.1002/(SICI)1097-0207(19980215)41:3%3C541::AID-NME298%3E3.0.CO;2-K.
14. **Parreira, P.** 1988. On the accuracy of continuous and discontinuous boundary elements, Engineering Analysis 5: 205-211. https://doi.org/10.1016/0264-682X(88)90018-4.
15. **Cotter, C. J.; Ham, D. A.; Pain, C. C.** 2009. A mixed discontinuous/continuous finite element pair for shallow-water ocean modelling, Ocean Modelling 26(1-2): 86-90. https://doi.org/10.1016/j.ocemod.2008.09.002.
16. **Mukhopadhyay, S.; Majumdar, N.** 2009. A study of three-dimensional edge and corner problems using the neBEM solver, Engineering Analysis with Boundary Elements 33(2); 105-119. https://doi.org/10.1016/j.enganabound.2008.06.003.
17. **Zhang, J.; Zhong, Y.; Dong, Y.; Lin, W.** 2018. Expanding element interpolation method for analysis of thin-walled structures, Engineering Analysis with Boundary Elements 86: 82-88. https://doi.org/10.1016/j.enganabound.2017.10.014.
18. **Gao, X. W.; Yang, K.; Wang, J.** 2008. An adaptive element subdivision technique for evaluation of various 2D singular boundary integrals, Engineering analysis with boundary elements 32(8): 692-696. https://doi.org/10.1016/j.enganabound.2007.12.004.
19. **Johnston P R.; Elliott** D. 2001. A generalisation of Telles' method for evaluating weakly singular boundary element integrals, Journal of Computational and Applied Mathematics 131(1): 223-241. https://doi.org/10.1016/S0377-0427(00)00273-9.
20. **Zhong, Y. D.; Hou, J. J.; Feng, S. Z.; Xie, G.; Wang, X.; He, W.; Wang, L.; Chen, Z. Q.; Hao, H. W.** 2022. BEM analysis of multilayer thin structures using a composite transformation method for boundary integrals, Engineering Analysis with Boundary Elements 134: 650-664. https://doi.org/10.1016/j.enganabound.2021.11.007.
21. **Guiggiani, M.; Gigante, N.** 1990. A general algorithm for multi-dimensional Cauchy principal value integrals in the boundary element method, ASME Journal of applied Mechanics 57: 906-915. https://doi.org/10.1115/1.2897660.

22. **Sladek, V.; Sladek, J.; Tanaka, M.** 1993. Regularization of hypersingular and nearly singular integrals in the potential theory and elasticity, International Journal for Numerical methods in Engineering 36(10): 1609-1628. https://doi.org/10.1002/nme.1620361002.
23. **Niu, Z. R.; Wendland, W. L.; Wang, X. X.; Zhou, H. L.** 2005. A semi-analytic algorithm for the evaluation of the nearly singular integrals in three-dimensional boundary element methods, Computer Methods in Applied Mechanics and Engineering194(9-11): 1057-1074. https://doi.org/10.1016/j.cma.2004.06.024.
24. **Zhou, H. L.; Niu, Z. R.; Cheng, C. Z.; Guan, Z. W.** 2008. Analytical integral algorithm applied to boundary layer effect and thin body effect in BEM for anisotropic potential problems, Computers & structures 86(15-16): 1656-1671. https://doi.org/10.1016/j.compstruc.2007.10.002.
25. **Zhang, J. M.; Lu, C. J.; Zhang, X. X.; Xie, G. Z.; Dong, Y. Q; Li, Y.** 2015. An adaptive element subdivision method for evaluation of weakly singular integrals in 3D BEM, Engineering Analysis with Boundary Elements 51: 213-219. https://doi.org/10.1016/j.enganabound.2014.11.002.
26. **Gao, X. W.; Zhang, J. B.; Zheng, B. J.; Zhang, C.** 2016. Element-subdivision method for evaluation of singular integrals over narrow strip boundary elements of thin-walled and slender structures, Engineering Analysis with Boundary Elements. 66: 145-154. https://doi.org/10.1016/j.enganabound.2016.02.002.
27. **Zhang, Y.; Gong, Y.; Gao, X.** 2015. Calculation of 2D nearly singular integrals over high-order geometry elements using the sinh transformation, Engineering Analysis with Boundary Elements. 60: 144-153. https://doi.org/10.1016/j.enganabound.2014.12.006.
28. **Gu, Y.; Zhang, C. Z.** 2021. Fracture analysis of ultrathin coating/substrate structures with interface cracks, International Journal of Solids and Structures 225: 111074. https://doi.org/10.1016/j.ijsolstr.2021.111074.
29. **Hayami, K.** 2005. Variable Transformations for Nearly Singular Integrals in the Boundary Element Method, Publications of the Research Institute for Mathematical Sciences 41(4): 821-842. https://doi.org/10.2977/prims/1145474596.
30. **Scuderi, L.** 2008. On the computation of nearly singular integrals in 3D BEM collocation, International Journal for Numerical Methods in Engineering 74(11): 1733-1770. https://doi.org/10.1002/nme.2229.
31. **Sladek, V.; Sladek, J.** 1998. Optimal coordinate transformations in numerical integrations of weakly singular and nearly singular integrals in BEMs, WIT Transactions on Modelling and Simulation 20: 233-242.
32. **Johnston, P.R.; Elliott, D.** 2005. A sinh transformation for evaluating nearly singular boundary element integrals, International journal for numerical methods in engineering 62(4): 564-578. https://doi.org/10.1002/nme.1208.
33. **Johnston, B. M.; Johnston, P. R.; Elliott, D.** 2007. A sinh transformation for evaluating two ‐ dimensional nearly singular boundary element integrals, International journal for numerical methods in engineering 69(7): 1460-1479. https://doi.org/10.1002/nme.1816.
34. **Poullikkas, A.; Karageorghis, A.; Georgiou, G.** 2002. The method of fundamental solutions for three-dimensional elastostatics problems, Computers & structures 80(3-4): 365-370. https://doi.org/10.1016/S0045-7949(01)00174-2.
35. **Aliabadi, F. M. H.** 2020. Boundary Element Methods, in Altenbach, H., Öchsner, A. (eds) Encyclopedia of continuum mechanics. Berlin, Heidelberg: Springer 182-193. https://doi.org/10.1007/978-3-662-55771-6_18.

Y. Zhong, X. Zeng, G. Xie, J. Hou, R. Wang, L. Wang, W. He

STRUCTURE ANALYSIS FOR PLATE COMPONENTS USING AN ADVANCED BOUNDARY ELEMENT METHOD

S u m m a r y

Accurate and effective evaluation of physical variables (displacement, traction, stress) of the plate structure is of great significance for the safety and stability of its design. In this paper, an advanced boundary element method is developed to perform the structure analysis for plate components with curve or thin features. The method is implemented as follows: Firstly, a novel interpolation method is developed to improve the simulation accuracy of the physical quantities on various structural models of plate components, which can improve the order of interpolation polynomials without changing the degrees of freedom of system equations, and eliminate the influence of the fitting error of physical variable in integral equation; And then an integral transformation frame is employed to remove the influence of the singular and nearly singular integrals in integral equation and ensure the accurate calculation of elastic parameters of plate components; Finally, several numerical examples (a porous plate, a deck framing and a propeller structure are included) are given to verify the feasibility of the proposed method. The results show that the proposed method can accurately evaluate the physical variables of the plate components.

Keywords: nearly singular integrals, structure analysis, plate components, boundary analysis, sinh transformation.

Received March 7, 2024
Accepted October 22, 2024